Superconductivity in the ternary germanide $La_3Pd_4Ge_4$

H. Fujii,[1] T. Mochiku,[1] H. Takeya,[1] and A. Sato[2]
[1]*Superconducting Materials Center, National Institute for Materials Science, 1-2-1 Sengen, Tsukuba, Ibaraki 305-0047, Japan*
[2]*Materials Analysis Station, National Institute for Materials Science, 1-1 Namiki, Tsukuba, Ibaraki 305-0044, Japan*
(Received 22 May 2005; revised manuscript received 14 September 2005; published 28 December 2005)

The ternary germanide $La_3Pd_4Ge_4$ has been prepared by arc melting. This compound takes a body-centered lattice with an orthorhombic unit cell with the lattice parameters of $a=4.2200(3)$ Å, $b=4.3850(3)$ Å, and c $=25.003(2)$ Å. The crystal structure of $La_3Pd_4Ge_4$ is $U_3Ni_4Si_4$-type with the space group of *Immm*, consisting of the combination of structural units of AlB_2-type and $BaAl_4$-type layers. This compound is a type-II superconductor with a critical temperature (T_c) of 2.75 K. The lower critical field $H_{c1}(0)$ is estimated to be 54 Oe. The upper critical field $H_{c2}(0)$ estimated by linear extrapolation of the $H_{c2}(T)$ curves is about 4.0 kOe, whereas the Werthamer-Hefland-Hohemberg theory gives $H_{c2}(0)^{WHH}=3.0$ kOe. This is an interesting observation of superconductivity in the compounds with $U_3Ni_4Si_4$-type structure. The coherence length $\xi(0)$ of 330 Å and the penetration depth $\lambda(0)$ of 2480 Å are derived.

DOI: 10.1103/PhysRevB.72.214520 PACS number(s): 74.70.Dd, 61.10.Nz, 68.37.Lp

I. INTRODUCTION

Among ternary intermetallic compounds, $ThCr_2Si_2$-type intermetallics, RET_2M_2 (RE=rare earth, T=transition metal, M=Si and Ge), have been extensively studied, especially for the interest of the superconducting and magnetic properties. The structure of $ThCr_2Si_2$ is the ordered ternary derivative of the binary $BaAl_4$-type structure.[1] Although superconductivity is observed for some compounds, the critical temperature (T_c) is as low as 1 K, as reported for $LaPd_2Ge_2$ and $LaPt_2Ge_2$ with T_cs of 1.12 and 0.55 K, respectively.[2] Many works were carried out for the discovery of different intermetallic superconductors with higher T_cs. Finally, quaternary intermetallic borocarbide superconductors RET_2B_2C with $ThCr_2Si_2$-derivative structure showing high T_cs were discovered.[3–6] Among these compounds, YPd_2B_2C shows a T_c of 23 K, which is the highest among $ThCr_2Si_2$-type intermetallic compounds.

Apart from $ThCr_2Si_2$-type structure, another intermetallic superconductor, MgB_2, was discovered several years ago.[7] The MgB_2 shows a T_c as high as 39 K, which is the highest among intermetallic compounds. The structure of the MgB_2 is AlB_2-type structure, which is composed of alternating hexagonal layers of Al atoms and graphitelike honeycomb layers of B atoms. Many works have been done so far on the compounds with AlB_2-type structure after the discovery of MgB_2, and several superconductors with this structure have been reported.[8,9] In this paper we report a different ternary germanide superconductor, $La_3Pd_4Ge_4$.

II. EXPERIMENT

Starting materials were La (chunk, 99.9% in purity), Pd (sheet, 99.99%), and Ge (granule, 99.999%). They were arc melted with a stoichiometric ratio of $La_3Pd_4Ge_4$ under Ar gas atmosphere on a water-cooler copper hearth. The melting was repeated several times with the button turned over between each melt. The weight loss was less than 1%. After melting, the obtained button wrapped in a Mo foil was annealed in an evacuated silica tube at 1173 K for one week.

Phase identification was carried out for crushed powder samples by an x-ray-diffraction (XRD) method with an x-ray diffractometer JEOL JDX-3500. The XRD patterns were fitted using the Rietveld refinement program RIETAN 2000.[10] Microstructural observation was carried out using a scanning electron microscope (SEM) with an energy dispersive x-ray (EDX) spectrometer. Electron diffraction (ED) patterns and high-resolution electron microscope (HREM) images were recorded for crushed samples using a JEOL JEM-4000EX. The crushed samples were dispersed in CCl_4 and transferred to carbon coated copper grids. Image calculations were carried out using a MACTEMPAS software program.

dc magnetization measurements were performed for bulk and crushed powder samples with a superconducting quantum interference device (SQUID) magnetometer, Quantum Design MPMS XL. *M-H* and *M-T* curves were recorded at temperatures above 1.8 K in fields up to 5 kOe. The volume fraction of the superconducting phase was estimated from the magnitude of zero-field-cooled (ZFC) magnetization in a field of 10 Oe in the *M-T* measurements. The T_c was defined as the onset temperature where a diamagnetic signal was observed. Electrical resistivity measurements were carried out in the temperature range from 1.8 to 300 K by a standard dc four-probe method.

III. RESULTS AND DISCUSSION

SEM-EDX analysis was performed on the polished cross section of the samples. The composition of the main phase in the samples was $La_3Pd_4Ge_4$. ED patterns taken along the various zone axes for the $La_3Pd_4Ge_4$ phase suggest that the $La_3Pd_4Ge_4$ takes an orthorhombic unit cell with the lattice parameters of $a=4.22$ Å, $b=4.39$ Å, and $c=25.0$ Å. The reflection condition was $h+k+l=2n$. These indicate that the lattice of the $La_3Pd_4Ge_4$ is body-centered with a suggested space group of $Imm2, I222, I2_12_12_1$, or *Immm*.

Most of the diffraction peaks in the XRD pattern were indexed on the basis of an orthorhombic unit cell with the

TABLE I. The atomic parameters for $La_3Pd_4Ge_4$. g is the occupancy factor.

Atom	Site	x	y	z	g	B (Å^2)
La(1)	2a	0	0	0	1.0	1.0
La(2)	4j	0.50	0	0.3513(2)	1.0	1.0
Pd(1)	4j	0.50	0	0.0979(2)	1.0	1.0
Pd(2)	4i	0	0	0.2501(2)	1.0	1.0
Ge(1)	4j	0.50	0	0.1972(2)	1.0	1.0
Ge(2)	4i	0	0	0.4503(3)	1.0	1.0

lattice parameters of $a=4.2200(3)$ Å, $b=4.3850(3)$ Å, and $c=25.003(2)$ Å. This is in agreement with the lattice parameters obtained from the ED patterns. Other small peaks could be indexed on the basis of a tetragonal unit cell of $LaPd_2Ge_2$ with the space group of $I4/mmm$ with the lattice parameters of $a=4.3692(9)$ Å and $c=10.023(2)$ Å. These lattice parameters of the $LaPd_2Ge_2$ are slightly smaller than those reported previously.[11] Although some shiny crystals were observed in the crushed samples, they were identified as $LaPd_2Ge_2$ single crystal.

Analog compounds, $La_3Rh_4Ge_4$ and $Ce_3Rh_4Ge_4$, take $U_3Ni_4Si_4$-type structure with an orthorhombic unit cell with the space group of *Immm*.[12,13] The lattice parameters of $La_3Rh_4Ge_4$ are $a=4.1746(3)$ Å, $b=4.2412(2)$ Å, and $c=25.234(3)$ Å, whereas the lattice parameters of $Ce_3Rh_4Ge_4$ are $a=4.0915(5)$ Å, $b=4.2400(19)$ Å, and $c=25.0673(82)$ Å. These parameters are almost equal to those of $La_3Pd_4Ge_4$. Therefore the crystal structure of $La_3Pd_4Ge_4$ was refined on the basis of the $U_3Ni_4Si_4$-type structural model with the space group of *Immm*. The Rietveld refinements for the XRD patterns were carried out for $La_3Pd_4Ge_4$ and $LaPd_2Ge_2$ simultaneously. Tables I and II list the final results of the refinements for $La_3Pd_4Ge_4$. The atomic parameters are listed in Table I, and the lattice parameters and the R factors[14] are listed in Table II. The volume fractions of the $La_3Pd_4Ge_4$ and $LaPd_2Ge_2$ were estimated to be 96 and 4 %, respectively. Figure 1 illustrates the observed, the calculated, and the difference pattern. The final R_{wp} factor was 15.06%. This relatively high R_{wp} factor may be due to the presence of impurity phases other than $LaPd_2Ge_2$. The presence of the $LaPd_2Ge_2$ and the weight loss less than 1% after arc melting suggest the presence of a small amount of other impurity phases. The XRD peaks of the other impurity phases may overlap those of the $La_3Pd_4Ge_4$ and $LaPd_2Ge_2$.

TABLE II. The lattice parameters and the R factors for $La_3Pd_4Ge_4$.

a (Å)	4.2200(3)
b (Å)	4.3850(3)
c (Å)	25.003(2)
V (Å^3)	462.67(5)
R_{wp} (%)	15.06
R_p (%)	11.85
R_R (%)	20.81
R_I (%)	6.91
R_F (%)	6.04
R_e (%)	7.60
S	1.98

The isotropic thermal parameters B of all the atoms in the $La_3Pd_4Ge_4$ were fixed at 1.0 for the fitting, because the refinement of those B parameters caused not only smaller $R_{wp}(\approx 14\%)$ but also $B<0$. The structural refinements on the basis of other space groups were not successful. Therefore the $U_3Ni_4Si_4$-type structure with the space group of *Immm* is probably the most suitable for $La_3Pd_4Ge_4$.

A [010] HREM image of $La_3Pd_4Ge_4$ is shown in Fig. 2. Here the corresponding ED pattern and calculated image are together shown in the inset. The image calculations were carried out with the results of the refinements listed in Tables I and II. The calculated image along the [010] zone axis was obtained with $(\Delta f, t)=(-760\ \text{Å}, 18\ \text{Å})$. Here Δf and t denote defocus values and specimen thickness, respectively. In the experimental image, regular structure along the c axis with

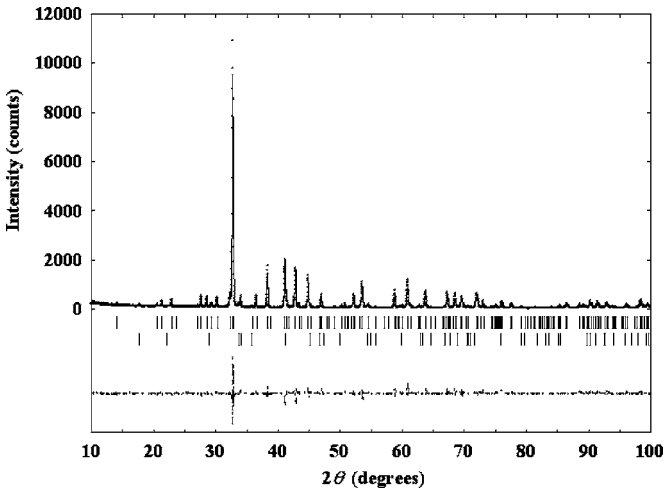

FIG. 1. Observed, calculated, and difference x-ray-diffraction data for $La_3Pd_4Ge_4$. Plus marks (+) and the overlapped continuous line indicate the observed diffraction data and the calculated pattern, respectively. The refinement was carried out on the basis of $U_3Ni_4Si_4$-type structural model with the space group of *Immm*. The background was fitted as a part of the refinement. The upper and lower vertical lines below the pattern denote the peak positions of $La_3Pd_4Ge_4$ and $LaPd_2Ge_2$, respectively. The difference between observed and calculated intensities is shown at the bottom in the same scale.

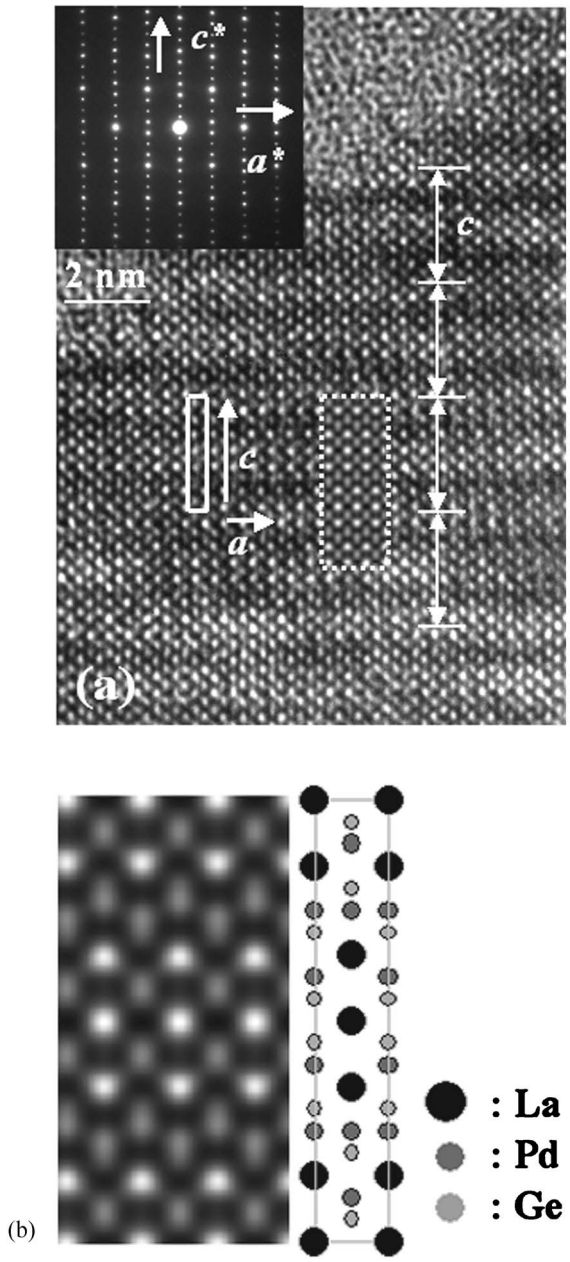

FIG. 2. (a) A HREM image taken along the [010] zone axis for $La_3Pd_4Ge_4$. The corresponding ED pattern and calculated image are shown in the inset. The unit cell and calculated image of $La_3Pd_4Ge_4$ are indicated by solid and dashed lines, respectively, in the experimental image. Regular structure with the periodicity of 25 Å along the c axis is observed. The calculated image was obtained with $(\Delta f, t) = (-760\ \text{Å}, 18\ \text{Å})$. Here Δf and t denote defocus values and specimen thickness, respectively. (b) The enlarged calculated image and a schematic view of the structure along the [010] zone axis for $La_3Pd_4Ge_4$. The La atom is imaged as large white dots, whereas the Pd and Ge atoms are merged as ellipsoidal gray dots.

the periodicity of 25 Å is clearly observed, and no irregular intergrowth of blocks is observed. This is in agreement with the corresponding ED pattern where no streaks along the c^* axis are observed. Compared with the experimental and calculated images, the calculated image is in good agreement with the corresponding experimental image. With the results

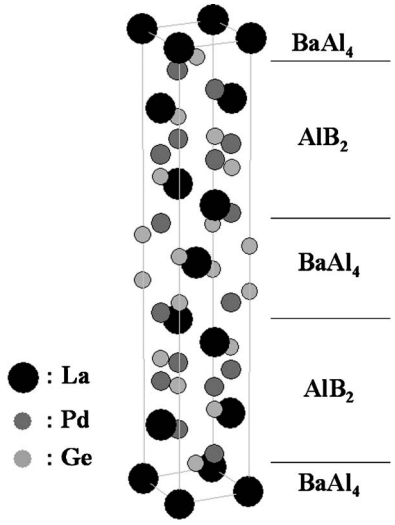

FIG. 3. Crystal structure of $La_3Pd_4Ge_4$. Here La, Pd, and Ge are denoted by large, medium, and small circles, respectively.

of the Rietveld refinements mentioned above, we conclude that the crystal structure of $La_3Pd_4Ge_4$ is $U_3Ni_4Si_4$ type with the space group of *Immm*.

Figure 3 shows the crystal structure of $La_3Pd_4Ge_4$. This structure is composed of combination of structural units of AlB_2-type and $BaAl_4$-type layers according to the relation $2La(Pd_{0.5}Ge_{0.5})_2 + LaPd_2Ge_2 = La_3Pd_4Ge_4$. The $U_3Ni_4Si_4$-type structure is observed for other related compounds, $R_3Rh_4Ge_4$ (R=La and Ce), as mentioned above. On the other hand, $Ln_3Pd_4Ge_4$ (Ln=Y, Gd-Yb) takes the same body-centered lattice with the orthorhombic unit cell with the space group of *Immm*, but the structure is not $U_3Ni_4Si_4$ type but $Gd_3Cu_4Ge_4(Li_4Sr_3Sb_4)$ type.[15–20] Whereas the size of La is large and its atomic radius is 1.87 Å, the atomic radii of *Ln* are smaller than that of La due to lanthanide contraction. The atomic radii of *Ln* are too small to form $U_3Ni_4Si_4$-type structure.

Both $U_3Ni_4Si_4$-type and $Gd_3Cu_4Ge_4(Li_4Sr_3Sb_4)$-type structures contain structural units of AlB_2-type layers. The essential difference between these structures is the coordination of the Ni and Cu. In $La_3Pd_4Ge_4$, only the Pd atoms in the $BaAl_4$ layers are tetrahedrally surrounded by Ge atoms, whereas other Pd atoms in the AlB_2 layers are surrounded by three Ge atoms in a trigonal planar configuration. On the other hand, in $Ln_3Pd_4Ge_4$ with $Li_4Sr_3Sb_4$-type structure, all the Pd atoms are located in the center of a tetrahedron of Ge.

Figure 4 shows temperature-dependent dc magnetization measured in a field of 10 Oe both in ZFC and field-cooled (FC) modes for $La_3Pd_4Ge_4$. For the bulk sample, the diamagnetic signals are observed at 2.75 K for both modes with a 10–90 % transition width of about 0.2 K. The magnitude of magnetic shielding signal after being corrected for demagnetization effects is approximately equal to 100% of that estimated for perfect diamagnetism, while the magnitude of flux expulsion (Meissner effect) is approximately 5% of that estimated for perfect diamagnetism. The hysteresis observed between the signals in ZFC and FC modes indicates that this compound is a type-II superconductor.

The same dc magnetization measurements were carried out for finely crushed powder samples. This is also shown in

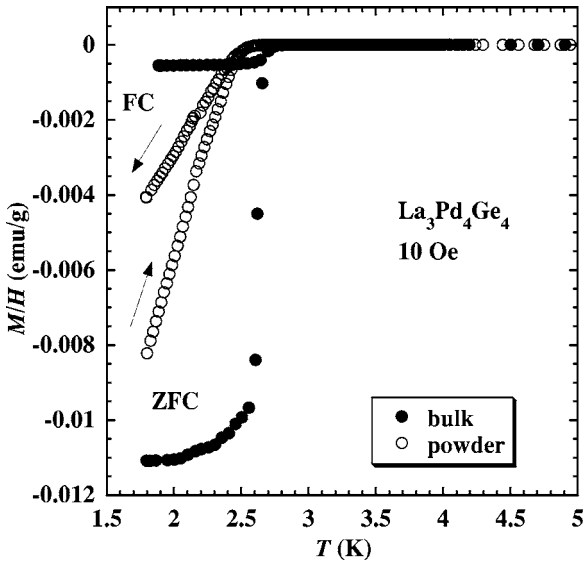

FIG. 4. Temperature-dependent dc magnetization curves for $La_3Pd_4Ge_4$. The data were recorded in zero-field cooled (ZFC) and field cooled (FC) modes for the bulk and powder samples. The applied field was 10 Oe.

Fig. 4. Compared with the result obtained for the bulk sample, the powder samples show a slightly lower T_c with broader transition and the magnitude of the FC magnetization is much larger. The magnitude of flux expulsion at 1.8 K is about half that of the ZFC magnetization. This difference is due to the magnetic flux trapping by the absence of a weak-link problem.[21] In the state of fine powder, the magnetic flux is easily expelled from the sample, resulting in the large Meissner effect. This indicates that the diamagnetic signal is due to the bulk superconductivity. The broadening of the transition observed for the powder sample is also reported for other compounds.[21,22]

Figure 5 shows the field dependence of magnetization curves $M(H)$ measured for the bulk sample at various temperatures. The details of the same curves in the background region are shown in the inset. These curves are characteristic for type-II superconductors. Figure 6 shows the temperature dependence of magnetization curves $M(T)$ measured for the bulk sample at various magnetic fields. The details of the same curves in the vicinity of T_c are also shown in the inset. Small kinks observed in the $M(T)$ curves at around 2.2 K are due to the temperature instability of the SQUID magnetometer.

The apparent lower critical field (H_{c1}^*)of the $La_3Pd_4Ge_4$ was determined by low-field magnetization measurements. H_{c1}^* at various temperatures was taken as the point of deviation of $M(H)$ from the linear M-H behavior observed at low magnetic fields. The true lower critical field (H_{c1}) was obtained from the H_{c1}^* by applying the correction for the demagnetization factor. The H_{c1} as a function of temperature is shown in Fig. 7. Fitting with the formula $H_{c1} = H_{c1}(0)[1-(T/T_c)^2]$ results in $H_{c1}(0)=54$ Oe. The $H_{c1}(0)$ is much lower than that of intermetallic Ni-based borocarbide superconductors (around 800 Oe) (Ref. 23) and MgB_2 (around 400 Oe).[24]

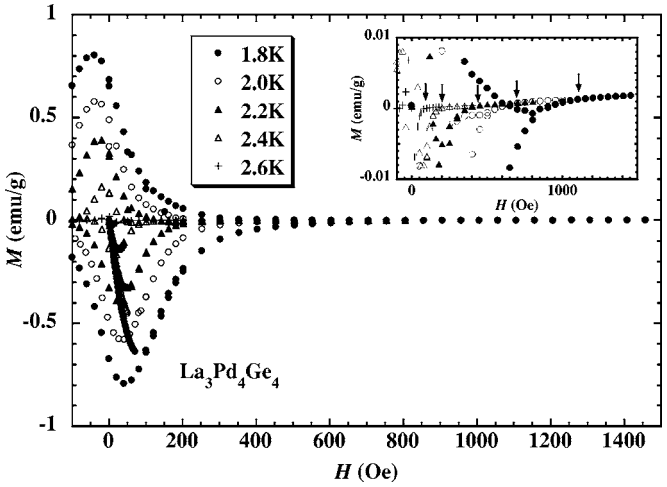

FIG. 5. Field dependence of magnetization curves $M(H)$ at various temperatures for $La_3Pd_4Ge_4$. The details of the same curves in the background region are shown in the inset. The points where the $M(H)$ curves reach the background are indicated by arrows for each temperature.

The upper critical field (H_{c2}) was estimated from both $M(H)$ and $M(T)$ curves. For the $M(H)$ curves, the H_{c2} was determined from the point where the $M(H)$ curves reach the background. For the $M(T)$ curves, the H_{c2} was estimated, taking account of the onset point of superconducting transition of the $M(T)$ curves. The H_{c2} estimated from these curves as a function of temperature is shown in Fig. 8.

Both $H_{c2}(T)$ curves obtained from the $M(H)$ and $M(T)$ curves show a positive curvature in the vicinity of T_c, similar to other superconductors, such as Li_2Pd_3B (Ref. 22) and borocarbides.[23] Except for this region, the gradient $-dH_{c2}/dT$ is estimated to be 1.6 kOe/K for both $H_{c2}(T)$ curves. These values are comparable to those reported for other ternary rare-earth transition-metal silicides and ger-

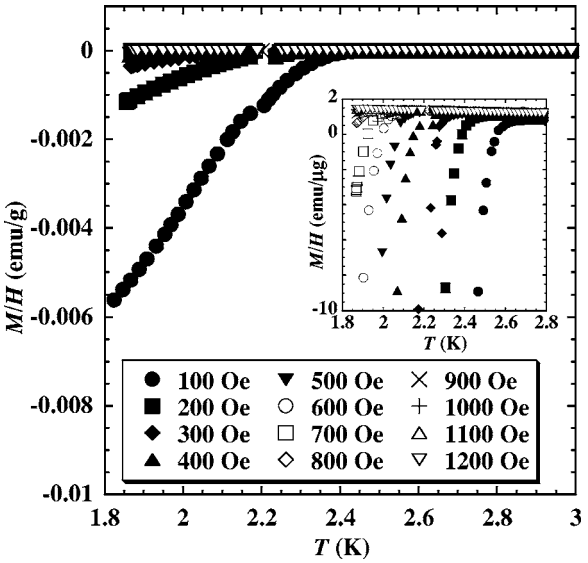

FIG. 6. Temperature dependence of magnetization curves $M(T)$ at various magnetic fields. The details of the same curves in the vicinity of T_c are shown in the inset.

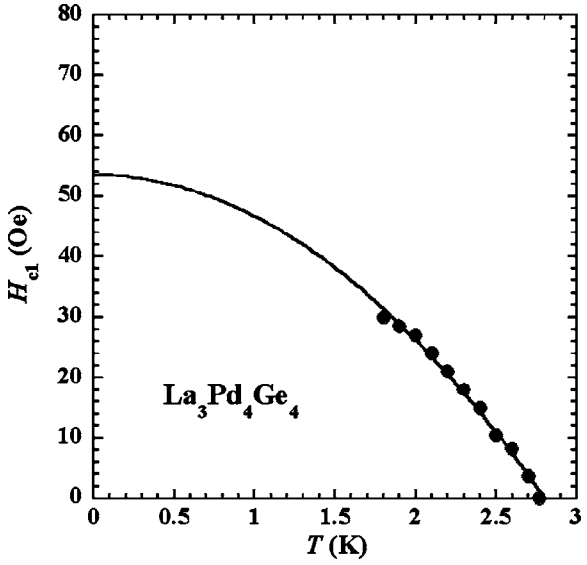

FIG. 7. Lower critical field H_{c1} as a function of temperature. The H_{c1} data are fitted with the formula $H_{c1}=H_{c1}(0)[1-(T/T_c)^2]$.

manides with low T_cs, such as $RE_5T_4X_{10}$ (RE=rare earth, T =transition metal, X=Si or Ge).[25] Linear extrapolation of the $H_{c2}(T)$ curves obtained from the $M(H)$ and $M(T)$ curves gives $H_{c2}(0)^{M\text{-}H}$=4.0 kOe and $H_{c2}(0)^{M\text{-}T}$=4.1 kOe, respectively. On the other hand, assuming the Werthamer-Hefland-Hohemberg (WHH) formula $H_{c2}(0)^{WHH}=-0.69T_c(dH_{c2}/dT)_{Tc}$,[26,27] $H_{c2}(0)^{WHH}$ of 3.0 kOe is obtained from both $H_{c2}(T)$ curves. In the following calculations, we have used $H_{c2}(0)^{WHH}$ for $H_{c2}(0)$.

With the formula $H_{c2}=\Phi_0/2\pi\xi^2$ (Φ_0 the flux quantum), the coherence length $\xi(0)$ is estimated to be 330 Å. This value is several times larger than those of borocarbide

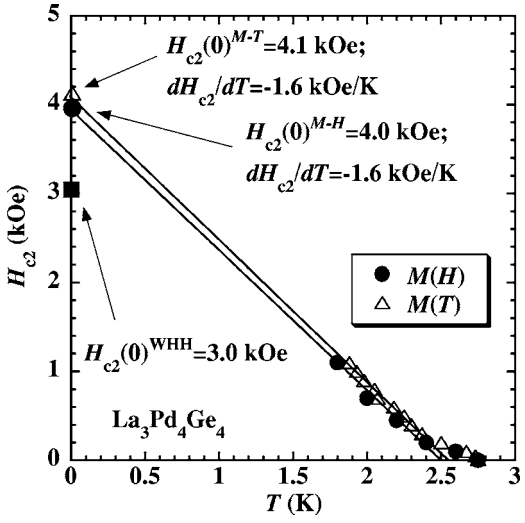

FIG. 8. Upper critical field H_{c2} obtained from $M(H)$ and $M(T)$ curves as a function of temperature. The $H_{c2}(0)^{M\text{-}H}$ and $H_{c2}(0)^{M\text{-}T}$ denoted by a solid circle and an open triangle are estimated by linear extrapolation of the $H_{c2}(T)$ curves obtained from the $M(H)$ and $M(T)$ curves, respectively. The $H_{c2}(0)^{WHH}$ estimated by the WHH formula is denoted by a solid square.

TABLE III. Measured and derived superconducting parameters for $La_3Pd_4Ge_4$.

T_c (K)	2.75
$H_c(0)$ (Oe)	280
$H_{c1}(0)$ (Oe)	54
$H_{c2}(0)$ (kOe)	3.0
$\lambda(0)$ (Å)	2480
$\xi(0)$ (Å)	330
$\kappa(0)$	7.5

superconductors[5,23] and MgB_2.[24] From $H_{c2}(0)$ and $\xi(0)$, the penetration depth $\lambda(0)$ is calculated to be 2480 Å with the formula $H_{c1}=(\Phi_0/4\pi\lambda^2)\ln(\lambda/\xi)$. This value is comparable to that of Pt-based borocarbide superconductors[5] and a few times larger than that of MgB_2.[24] The Ginzburg-Landau parameter $\kappa(0)$ is 7.5, derived from the formula $\kappa(0)=\lambda(0)/\xi(0)$, and thermodynamic critical field $H_c(0)$ is 280 Oe with the formula of $H_c(0)=H_{c2}(0)/\sqrt{2}\kappa(0)$. Table III lists these measured and derived superconducting parameters.

The electrical resistivity ρ as a function of temperature for $La_3Pd_4Ge_4$ is shown in Fig. 9. The detail of the region in the vicinity of T_c is shown in the inset. The resistivity decreases with decreasing temperature, showing metallic-type conductivity. The onset temperature of the transition is 2.85 K, and zero resistance is observed at 2.75 K. From 300 to 20 K, the temperature-dependent resistivity curve shows a small negative curvature. The room temperature resistivity, ρ(300 K), is approximately 270 $\mu\Omega$cm, and the residual resistivity, ρ(res), just above T_c, is 11 $\mu\Omega$cm. The resistivity residual resistivity ratio (RRR) is $\rho(300\text{ K})/\rho(\text{res})=24.5$. Such a small negative curvature and relatively high RRR are also reported for other ternary superconducting germanides such as $Y_5Rh_4Ge_{10}$.[25]

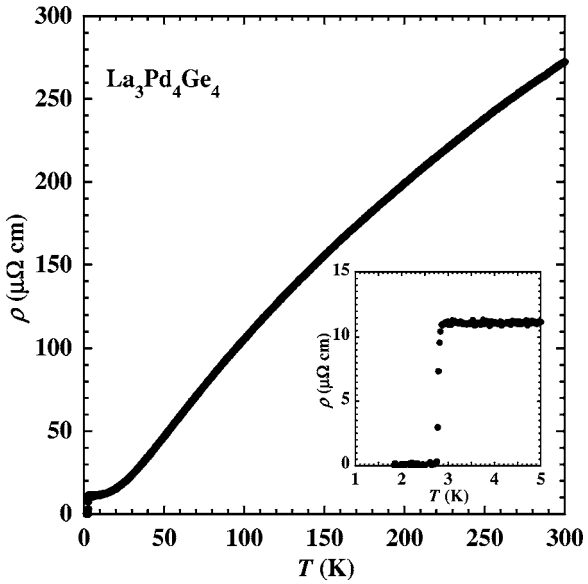

FIG. 9. Temperature-dependent electrical resistivity ρ for $La_3Pd_4Ge_4$. The detail of the region in the vicinity of T_c is shown in the inset.

IV. CONCLUSIONS

We have prepared ternary germanide $La_3Pd_4Ge_4$ by arc melting. The crystal structure of this compound is $U_3Ni_4Si_4$ type with the space group of *Immm*, consisting of combination of structural units of AlB_2-type and $BaAl_4$-type layers. The lattice parameters of the $La_3Pd_4Ge_4$ are $a=4.2200(3)$ Å, $b=4.3850(3)$ Å, and $c=25.003(2)$ Å. dc magnetization and electrical resistivity measurements indicated that the $La_3Pd_4Ge_4$ is a type-II superconductor with a T_c of 2.75 K. The lower critical field $H_{c1}(0)$ is 54 Oe. The upper critical fields $H_{c2}(0)$ estimated by linear extrapolation of the $H_{c2}(T)$ curves obtained from the $M(H)$ and $M(T)$ curves give $H_{c2}(0)^{M\text{-}H}=4.0$ kOe and $H_{c2}(0)^{M\text{-}T}=4.1$ kOe, respectively. On the other hand, the WHH theory gives $H_{c2}(0)^{\mathrm{WHH}}=3.0$ kOe.

[1] Z. Ban and M. Sikirica, Acta Crystallogr. **18**, 594 (1965).
[2] G. W. Hull, J. H. Wernick, T. H. Geballe, J. V. Waszczak, and J. E. Bernardini, Phys. Rev. B **24**, 6715 (1981).
[3] R. J. Cava, H. Takagi, B. Batlogg, H. W. Zandbergen, J. J. Krajewski, W. F. Peck, Jr., R. B. van Dover, R. J. Felder, T. Siegrist, K. Mizuhashi, J. O. Lee, H. Eisaki, S. A. Carter, and S. Uchida, Nature (London) **367**, 146 (1994).
[4] R. J. Cava, H. Takagi, H. W. Zandbergen, J. J. Krajewski, W. F. Peck, Jr., T. Siegrist, B. Batlogg, R. B. van Dover, R. J. Felder, K. Mizuhashi, J. O. Lee, H. Eisaki, and S. Uchida, Nature (London) **367**, 252 (1994).
[5] R. J. Cava, B. Batlogg, T. Siegrist, J. J. Krajewski, W. F. Peck, Jr., S. Carter, R. J. Felder, H. Takagi, and R. B. van Dover, Phys. Rev. B **49**, 12384 (1994).
[6] H. Fujii, S. Ikeda, T. Kimura, S-i. Arisawa, K. Hirata, H. Kumakura, K. Kadowaki, and K. Togano, Jpn. J. Appl. Phys., Part 2 **33**, L590 (1994).
[7] J. Nagamatsu, N. Nakagawa, T. Muranaka, Y. Zenitani, and J. Akimitsu, Nature (London) **410**, 63 (2001).
[8] A. S. Cooper, E. Corenzwit, L. D. Longinotti, B. T. Matthias, and W. H. Zachariasen, Proc. Natl. Acad. Sci. U.S.A. **67**, 313 (1970).
[9] M. Imai, E. Abe, J. Ye, K. Nishida, T. Kimura, K. Honma, H. Abe, and H. Kitazawa, Phys. Rev. Lett. **87**, 077003 (2001).
[10] F. Izumi and T. Ikeda, Mater. Sci. Forum **321-324**, 198 (2000).
[11] D. Rossi, R. Marazza, and R. Ferro, J. Less-Common Met. **66**, P17 (1979).
[12] E. Hovestreydt, K. Klepp, and E. Parthé, Acta Crystallogr., Sect. B: Struct. Crystallogr. Cryst. Chem. **38**, 1803 (1982).
[13] P. Rogl, B. Chevalier, and J. Etourneau, J. Solid State Chem. **88**, 429 (1990).
[14] R. A. Young, E. Prince, and R. A. Sparks, J. Appl. Crystallogr. **15**, 357 (1982).
[15] W. Rieger, Monatsch. Chem. **101**, 449 (1970).
[16] O. Liebrich, H. Schäfer, and A. Weiss, Z. Naturforsch. B **25**, 650 (1970).
[17] R. E. Gladyshevskii, O. L. Sologub, and E. Parthé, J. Alloys Compd. **176**, 329 (1991).
[18] Yu. M. Prots', O. I. Bodak, V. K. Pecharsky, P. S. Salamakha, and Yu. D. Seropegin, Z. Kristallogr. **205**, 331 (1993).
[19] P. Salamakha, O. Sologub, J. K. Yakinthos, and Ch. D. Routsi, J. Alloys Compd. **267**, 192 (1998).
[20] D. Niepmann, Y. M. Prots', R. Pöttgen, and W. Jeitschko, J. Solid State Chem. **154**, 329 (2000).
[21] R. J. Cava, H. W. Zandbergen, B. Batologg, H. Eisaki, H. Takagi, J. J. Krajewski, W. F. Peck, Jr., E. M. Gyorgy, and S. Uchida, Nature (London) **411**, 54 (2001).
[22] K. Togano, P. Badica, Y. Nakamori, S. Orimo, H. Takeya, and K. Hirata, Phys. Rev. Lett. **93**, 247004 (2004).
[23] H. Takagi, R. J. Cava, H. Eisaki, J. O. Lee, K. Mizuhashi, B. Batlogg, S. Uchida, J. J. Krajewski, and W. F. Peck, Jr., Physica C **228**, 389 (1994).
[24] C. Buzea and T. Yamashita, Supercond. Sci. Technol. **14**, R115 (2001).
[25] L. S. Hausermann-Berg and R. N. Shelton, Phys. Rev. B **35**, 4673 (1987).
[26] E. Helfand and W. R. Werthamer, Phys. Rev. **147**, 288 (1966).
[27] N. R. Werthamer, E. Helfand, and P. C. Hohemberg, Phys. Rev. **147**, 295 (1966).